Supporting Information For:

Homology Model of PMP22 Suggests Mutations Resulting In Peripheral Neuropathy Disrupt Transmembrane Helix Packing

Kathleen F. Mittendorf[†,‡], Brett M. Kroncke[†,‡], Jens Meiler[‡,§,#], and Charles R. Sanders[†,‡]*

[†]Department of Biochemistry, [‡]Center for Structural Biology, and [§]Departments of Pharmacology, and Bioinformatics, Vanderbilt University School of Medicine, Nashville, TN 37232, United States

[#]Dept. of Chemistry, Vanderbilt University, Nashville, TN 37232, United States

Contents:

Methods

Alignment. In this study, we used BCL::Align to generate an alignment of PMP22 (NP_696997.1) and the full sequence of murine claudin-15 (NP_068365.1). Following a previously published protocol, we weighted the PAM250 mutation matrix[1], PSIBLAST sequence profiles[2], PSIPRED secondary structure prediction[3], JUFO secondary structure prediction[4], and TMHMM transmembrane prediction[5] 0.25, 0.25, 0.15, 0.15, and 0.30, respectively. The gap opening and gap extension penalties were set to -3.0 and -0.3, respectively. The resulting alignment was trimmed to remove the cytosolic C-terminus of claudin-15 and the stretch of extracellular loop 1 (ECL1) residues (VHGNVITT) that was unresolved in the crystal structure (see Figure 1). The sequence of claudin-15 was also altered to include the cysteine-to-alanine mutations in the crystallized construct of claudin-15. The PMP22 TM regions and conserved "claudin motif" (W-[N/G/D]LW-C-C) in ECL1 (see text of main manuscript) aligned as expected with claudin-15 in light of the structure. To further verify the accuracy of the alignment generated by BCL::Align, the final alignment was compared to the results of HHPred, another alignment program that has proven successful for the alignment of membrane proteins[6,7,8], which predicts the exact same alignment for the TM regions, lending greater confidence to our initial model. The BCL::Align alignment guided the population of atoms into an initial PMP22 structure drawn from the claudin-15 coordinates using an in-house script (Jens Meiler, unpublished).

Loop rebuilding. Following building of the initial model, the following PMP22 residues were completely rebuilt using the loopmodel utility within Rosetta 3.5: 23-28, 30-33, 36-41, 44-51, 55-62, 86-93, and 119-134. These residues represent all elements not containing secondary structure as well as one flanking residue on each side of each secondary structure element. Fragment files were generated using the Rosetta server [9]. The loop building took place in two stages: (1) a low resolution "centroid" method that closes the loop and performs an initial relaxation (we used the default score4L centroid score function for soluble proteins at this stage since all loop-rebuilt residues reside in the soluble segment of PMP22 and since the soluble score function has been much more extensively benchmarked compared to the membrane-specific score function [10]), and (2) an all-atom refinement that allows side-chain and backbone conformational sampling of all loop residues, employing a membrane protein-specific scoring function; the score function used at this stage has been benchmarked with several membrane proteins and has recently performed well in discriminating native-like GPCR homology models [11]. The resulting conformation is then subjected to an energy minimization protocol that allows side-chain and backbone conformational sampling across the entire protein and is scored with a membrane protein-specific score function.

Relaxation, Clustering, and Evaluation of Models. The lowest scoring 1000 models, as evaluated by the full atom membrane protein-specific scoring function of Rosetta 3.5, were subjected to an additional round of relaxation—an energy minimization through iterative side-chain repacking and gradient-based minimization with a ramping repulsive potential ten times—each model producing 5 new structures for a total of 5000 new models. Of these 6000 total models, the top 1000 models were further relaxed, generating another 5000 new models. The final top-scoring 1000 models of all rounds were then clustered into structurally similar families using BCL::Cluster[12]. The top scoring models from the largest clusters (>20 members and having no further branchpoints) were chosen as the representative models; 26 in total. These top models were mutated to L16P, using the fixbb application within Rosetta, or left as wild type and further relaxed, generating 1000+ new models (40+ new models per starting model) for each variant. The best scoring 10 models for each variant were selected to generate the p-value. To calculate RMSD, all structures were compared to the most average/center model out of the 10 best scoring WT models. To generate Figure 2A and Figure S4, the final top-scoring 1000 models for WT were clustered into families as described above. These structures were aligned in Chimera (Figure 2A) or Pymol (Figure S4) and the RMSD to the top-scoring structure was calculated in UCSF Chimera (Figure 2A). The top-scoring structure represented in these clusters was utilized in all remaining figures of WT-PMP22 and is the structure described by the PDB file (for both wild type and the L16P mutant).

The top-scoring WT model was subjected to MolProbity analysis, which reported 152/160 (96.20%) residues were in favored regions of the Ramachandran plot, and 160/160 (100%) residues occupied allowed regions. Molprobity also reported a clashscore of 2.35 (99^{th} percentile), 1 poor rotamer (0.71%), no Cβ deviations, 0/1300 bad backbone bonds, and 4/1775 (0.23%) bad backbone angles. The MolProbity score was 1.27 (99^{th} percentile). Subsequent analysis presented in this paper, including the generation of all figures from a single model, was performed using this model. The pdb coordinates for this model are available for download as a part of the supporting information of this manuscript.

Similarly, the top-scoring L16P model was subjected to MolProbity analysis, which reported 152/160 (96.20%) residues were in favored regions of the Ramachandran plot, and 160/160 (100%) residues occupied allowed regions. Molprobity reported a clashscore of 3.92 (96^{th} percentile), 1 poor rotamer (0.71%), no Cβ deviations, 0/1300 bad backbone bonds, and 4/1775 (0.23%) bad backbone angles. The MolProbity score was 1.44 (96^{th} percentile). This model was then used as the basis for subsequent analysis presented in this paper, and is available for download as a part of the supporting information of this manuscript.

Because the above final models did not contain a disulfide bond, we repeated the analysis for WT to verify that adding a forced disulfide bond did induce gross alterations of predicted protein structure. The protocol followed to generate the disulfide-bonded models was identical to the above mentioned process with the addition of the fix_disulf flag and accompanying file listing the residues to be locked in a disulfide bond. After two relax iterations, clustering, and final relax step of the lowest energy cluster representative structures; the best scoring models had comparable values to those generated without the disulfide bond enforced--between -650 and -640 Rosetta energy units. To generate Figure S5, the overall backbone RMSDs between our original model and the top-scoring structure in each of these clusters were calculated. The nearest model, which is depicted in Figure S5, had an overall backbone RMSD of only 1.955 Å,

indicating very little changes are necessary to accommodate a disulfide bond restraint. This model was subjected to MolProbity analysis, which reported 151/160 (95.57%) residues were in favored regions of the Ramachandran plot, with 160/160 (100%) residues occupying allowed regions. Molprobity reported a clashscore of 2.35 (99th percentile), no poor rotamers, no Cβ deviations, 0/1300 bad backbone bonds, and 4/1775 (0.23%) bad backbone angles. The MolProbity score was 1.32 (98thpercentile). This model was then used as the basis for subsequent analysis presented in this paper, and is available as a Protein Databank file for download as a part of this SI.

Figure generation.

All protein structure figures were generated with The PyMOL Molecular Graphics System, Schrödinger, LLC, except Figure 2A, which was generated using UCSF Chimera version 1.9.[9]

Supporting References

[1] W.C. Barker, L.K. Ketcham, M.O. Dayhoff, A comprehensive examination of protein sequences for evidence of internal gene duplication, J Mol Evol 10 (1978) 265-281.

[2] S.F. Altschul, T.L. Madden, A.A. Schaffer, J. Zhang, Z. Zhang, W. Miller, D.J. Lipman, Gapped BLAST and PSI-BLAST: a new generation of protein database search programs, Nucleic Acids Res 25 (1997) 3389-3402.

[3] D.T. Jones, Protein secondary structure prediction based on position-specific scoring matrices, J Mol Biol 292 (1999) 195-202.

[4] J. Meiler, D. Baker, Coupled prediction of protein secondary and tertiary structure, Proc Natl Acad Sci U S A 100 (2003) 12105-12110.

[5] R.Y. Kahsay, G. Gao, L. Liao, An improved hidden Markov model for transmembrane protein detection and topology prediction and its applications to complete genomes, Bioinformatics 21 (2005) 1853-1858.

[6] M. Remmert, A. Biegert, A. Hauser, J. Soding, HHblits: lightning-fast iterative protein sequence searching by HMM-HMM alignment, Nature methods 9 (2012) 173-175.

[7] J. Soding, Protein homology detection by HMM-HMM comparison, Bioinformatics 21 (2005) 951-960.

[8] J. Soding, A. Biegert, A.N. Lupas, The HHpred interactive server for protein homology detection and structure prediction, Nucleic acids research 33 (2005) W244-248.

[9] D.E. Kim, D. Chivian, D. Baker, Protein structure prediction and analysis using the Robetta server, Nucleic Acids Res 32 (2004) W526-W531.

[10] C. Wang, P. Bradley, D. Baker, Protein-protein docking with backbone flexibility, J Mol Biol 373 (2007) 503-519.

[11] E.D. Nguyen, C. Norn, T.M. Frimurer, J. Meiler, Assessment and Challenges of Ligand Docking into Comparative Models of G-Protein Coupled Receptors, Plos One 8 (2013).

[12] N.W. Alexander, N.; Meiler, J., Bcl::Cluster: A method for clustering biological molecules coupled with visualization in the Pymol Molecular Graphics System, Computational Advances in Bio and Medical Sciences (ICCABS), 2011 IEEE 1st International Conference on, IEEE, 2011, pp. 13 - 18.

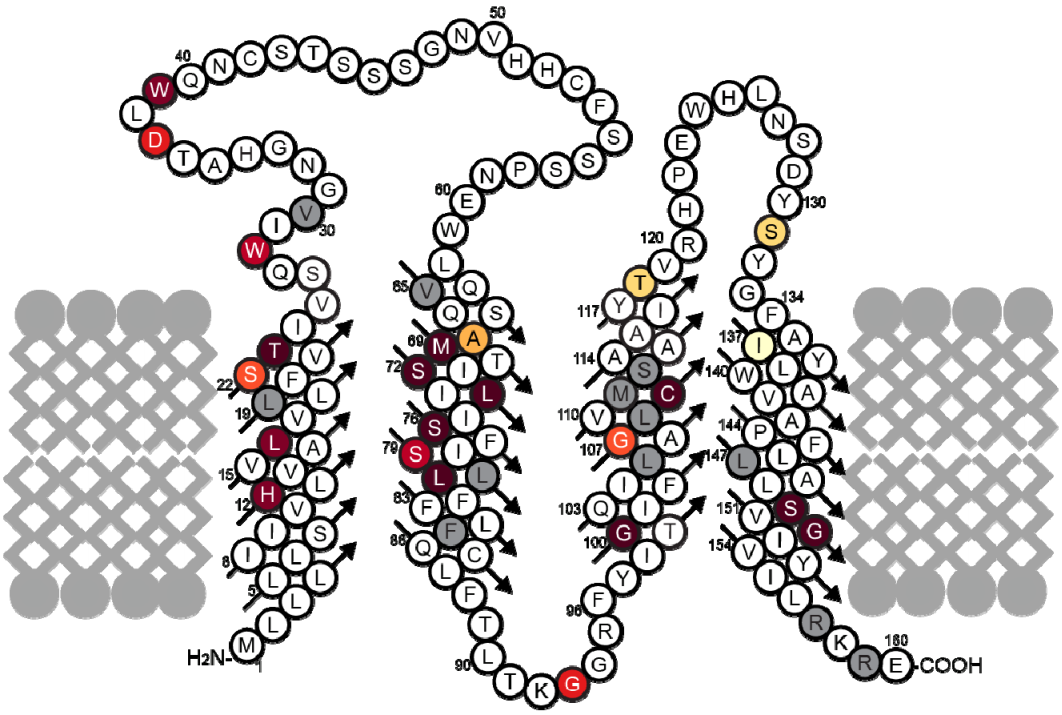

Figure S1. Topology diagram of PMP22. Known missense mutation sites are highlighted in red. Blue outlines represent disease mutations for which conduction velocities known (Figure 3, Table S1). The sequential spans of the helices match those of the model developed in this work. The extacellular loops (ECL1 and ECL2) are at the top and the intracellular loop (ICL1) is at the bottom of this figure.

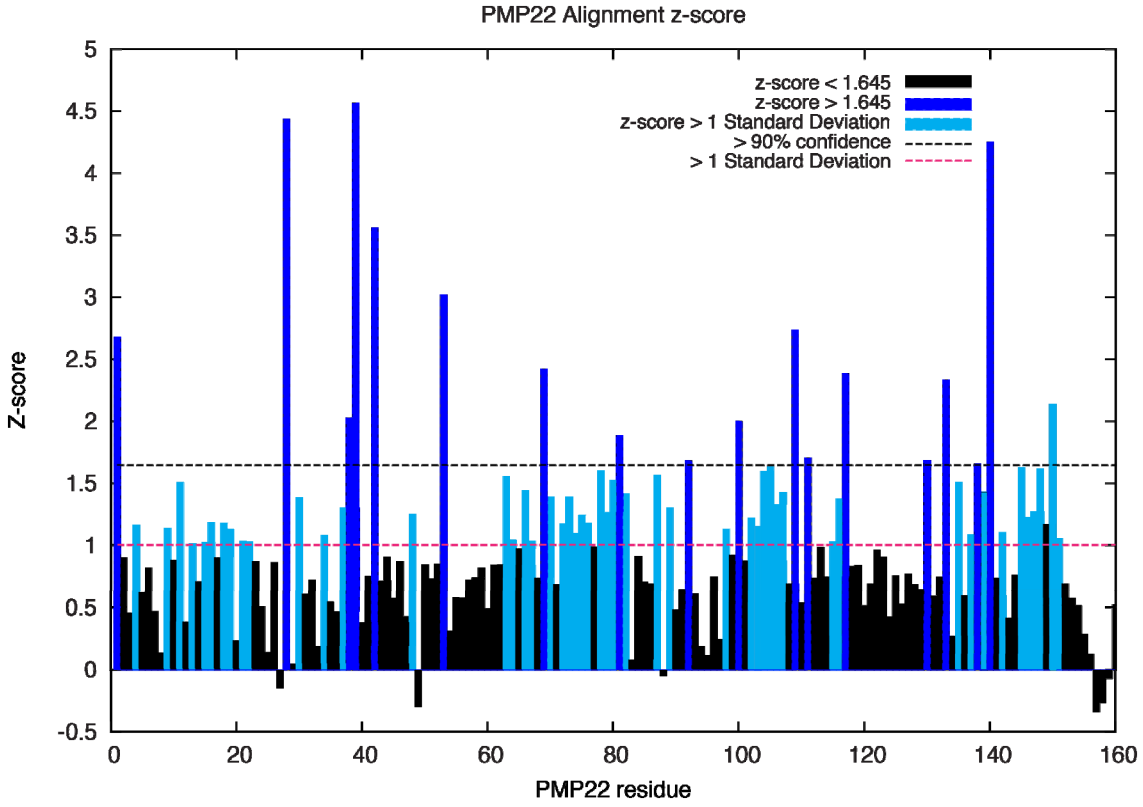

Figure S2. Per-residue z-scores generated by BCL::Align, depicting the confidence of the alignment. Note that residues with z-scores greater than 1.645 (>90% confidence) are spread throughout the sequence. Residues are numbered according to PMP22 residue number.

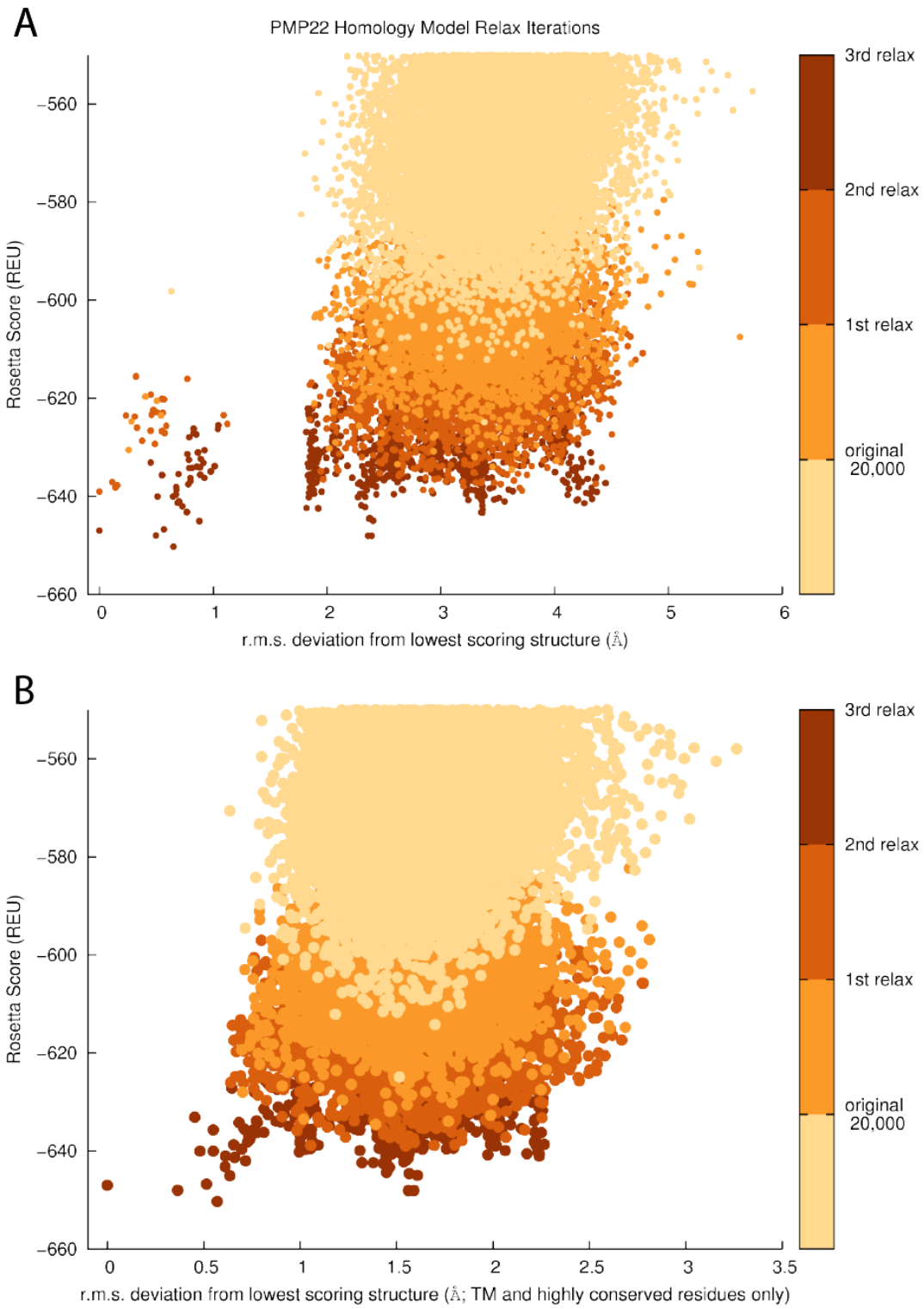

Figure S3. Rosetta energy score vs. RMSD from cluster center of final top 10 scoring PMP22 homology models for each iteration (see color key at right). (**A**) RMSD calculated using C_α positions from all residues in the PMP22 models. (**B**) RMSD calculated using C_α positions from TM and highly conserved residues only from PMP22 models

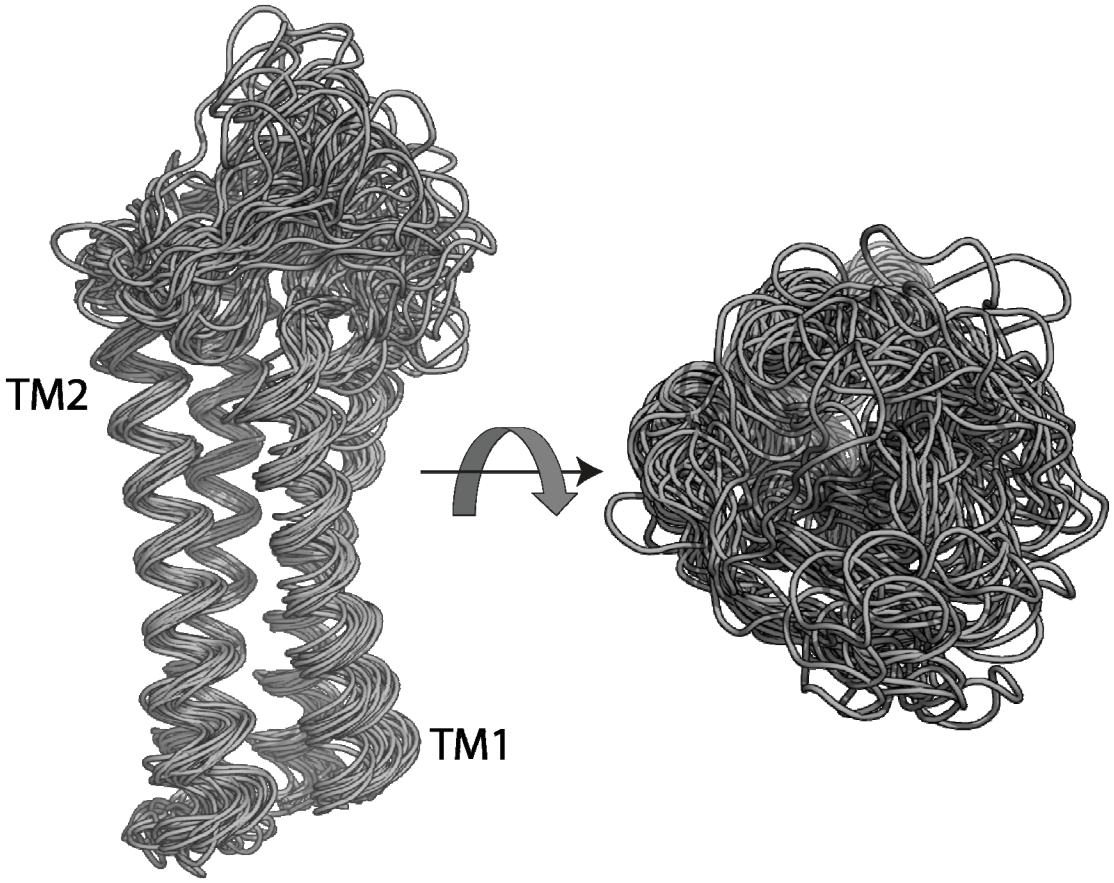

Figure S4. Overlay of the top scoring wild type PMP22 family member from each of 25 end-branch families with >20 members.

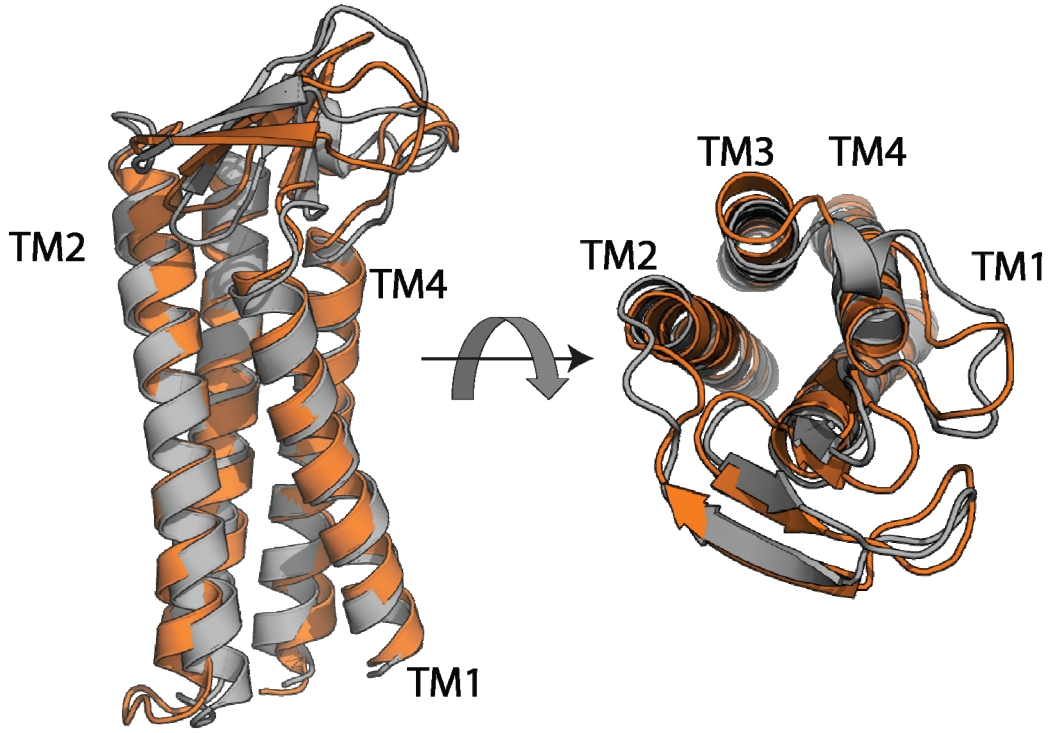

Figure S5. Final WT PMP22 homology model (grey) aligned to the nearest model (orange) from the top-scoring model containing a forced disulfide bond (see Methods section above), demonstrating the minimal changes (in the SS-free model) necessary to accommodate a disulfide bond (overall RMSD 1.955 Å). This suggests that our models are essentially the same whether or not a disulfide bond is present in PMP22 (a question that has not been addressed experimentally for native PMP22).

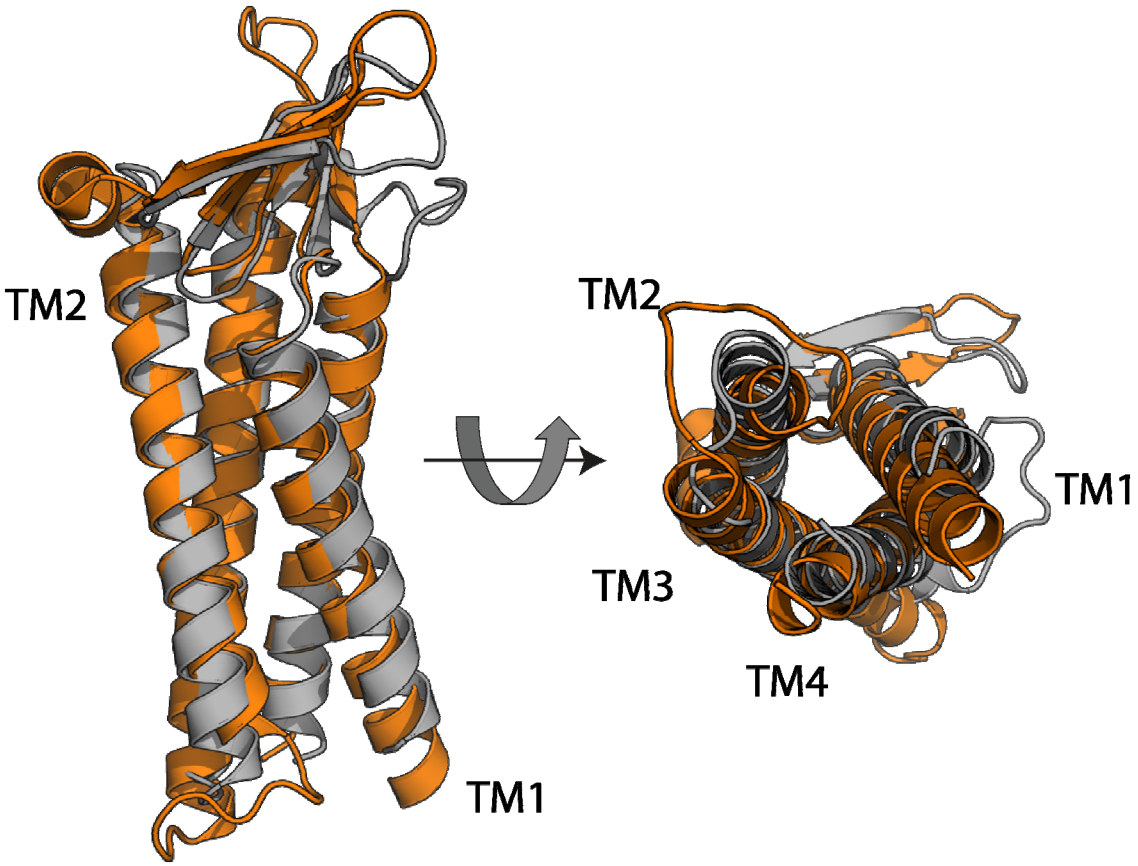

Figure S6. Final WT PMP22 homology model (grey) aligned to the crystal structure of murine claudin-15 (orange), demonstrating the slight outward rotation of TM1 and slight repacking of the TM interfaces that is seen in the final top scoring PMP22 models.

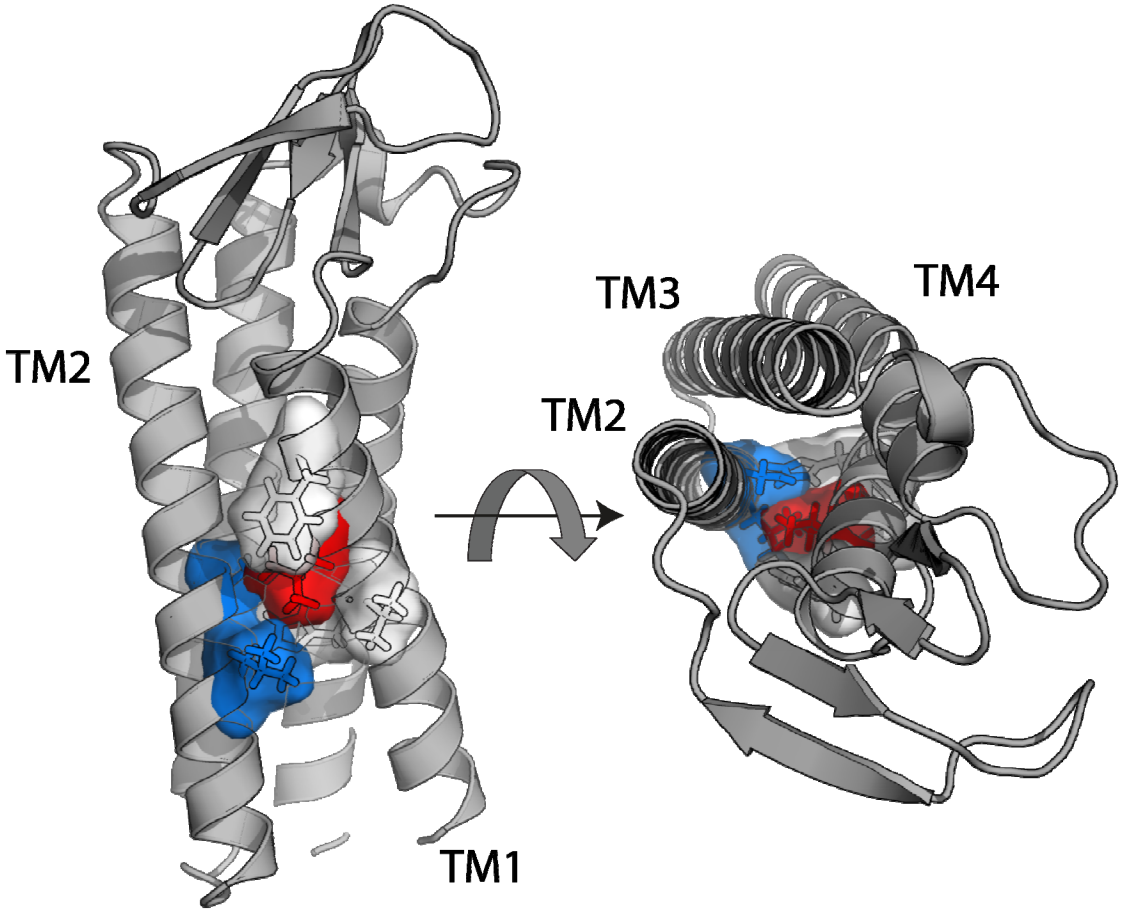

Figure S7. The WT PMP22 homology model indicates that L16 is essential for packing interactions of TM1 with TM2. L16 is displayed as sticks/surface and is colored red. The TM2 and TM1 residues in contact are displayed as sticks/surface and colored blue and white, respectively.

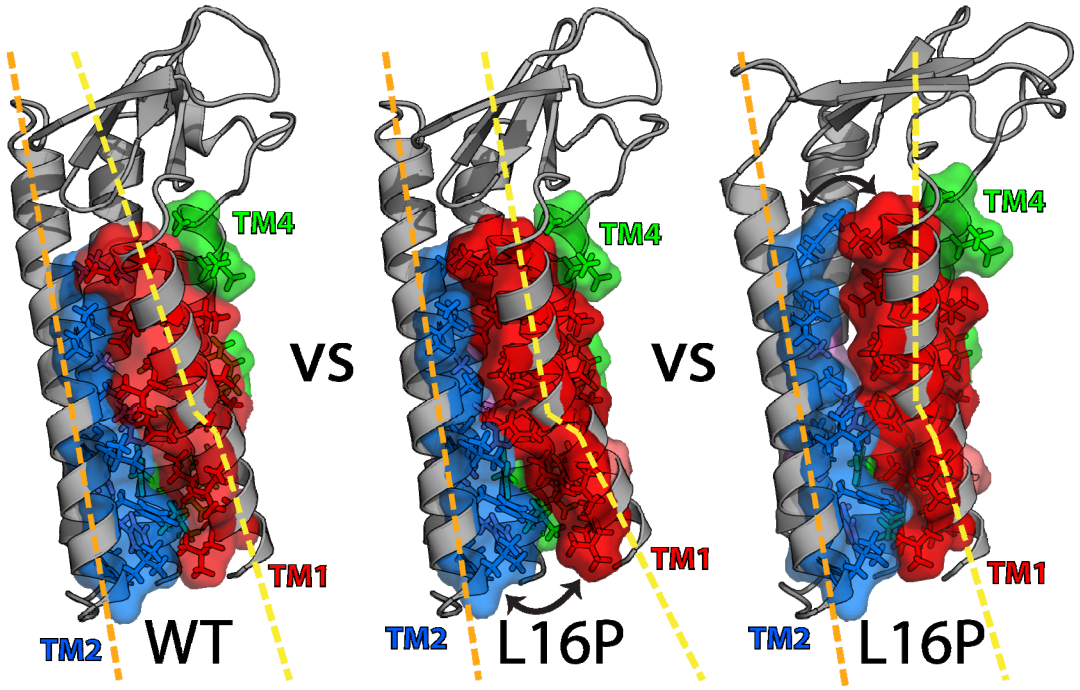

Figure S8. L16P mutation causes a reduced interface between TM1 and the rest of the helical bundle and a kink in the helix, consistent with reported experimental results. The WT model (left) shows a relatively straight TM1 that forms an interface with all TM helices. Two representative L16P models from the lowest scoring clusters (middle, lowest scoring model overall; right) demonstrate the kink in the helix (see line) and the reduced helical interface. Contacting residues of WT are colored red = TM1, marine = TM2, violet = TM3, and green = TM4 on all structures. Additional residues from TM1 on L16P making contacts are colored salmon.

Table S1. Patient motor nerve conduction velocities and literature references for each mutation depicted in Figure 3B of the paper.

PMP22 Mutation	Phenotype	Average Reported Motor Nerve Conduction Velocity (m/s)	Reference
H12Q	DSS	7	Hum Mutat. (1995) 5:76-80. Déjérine-Sottas neuropathy is associated with a de novo PMP22 mutation. Valentijn LJ, Ouvrier RA, van den Bosch NH, Bolhuis PA, Baas F, Nicholson GA.
L16P	CMT1	10	Identical point mutations of PMP-22 in Trembler-J mouse and Charcot-Marie-Tooth disease type 1A. Valentijn LJ, Baas F, Wolterman RA, Hoogendijk JE, van den Bosch NH, Zorn I, Gabreëls-Festen AW, de Visser M, Bolhuis PA. Nat Genet. (1992) 2:288-91 Allelic heterogeneity in hereditary motor and sensory neuropathy type Ia (Charcot-Marie-Tooth disease type 1a). Hoogendijk JE, Janssen EA, Gabreëls-Festen AA, Hensels GW, Joosten EM, Gabreëls FJ, Zorn I, Valentijn LJ, Baas F, Ongerboer de Visser BW, et al. Neurology. (1993) 43:1010-5.
S22F	HNPP/CMT1	25	A novel PMP22 mutation Ser22Phe in a family with hereditary neuropathy with liability to pressure palsies and CMT1A phenotypes. Kleopa KA1, Georgiou DM, Nicolaou P, Koutsou P, Papathanasiou E, Kyriakides T, Christodoulou K.Russo, Laura, 2011 Neuromuscul Disord Neurogenetics. (2004) 5:171-5. Variable phenotypes are associated with PMP22 missense mutations. Russo M, Laurá M, Polke JM, Davis MB, Blake J, Brandner S, Hughes RA, Houlden H, Bennett DL, Lunn MP, Reilly MM. Neuromuscul Disord. (2011) 21:106-14.
T23R	CMT1 and deafness	0	Variable phenotypes are associated with PMP22 missense mutations. Russo M, Laurá M, Polke JM, Davis MB, Blake J, Brandner S, Hughes RA, Houlden H, Bennett DL, Lunn MP, Reilly MM. Neuromuscul Disord. (2011) 21:106-14.
W28R	Severe CMT1 and deafness	13.7	Charcot-Marie-Tooth disease and related neuropathies: mutation distribution and genotype-phenotype correlation. Boerkoel CF, Takashima H, Garcia CA, Olney RK, Johnson J, Berry K, Russo P, Kennedy S, Teebi AS, Scavina M, Williams LL, Mancias P, Butler IJ, Krajewski K, Shy M, Lupski JR. Ann Neurol. (2002) 51:190-201.
D37V	Atypical CMT1	16.6	Myelin uncompaction in Charcot-Marie-Tooth neuropathy type 1A with a point mutation of peripheral myelin protein-22. Fabrizi GM, Cavallaro T, Taioli F, Orrico D, Morbin M, Simonati A, Rizzuto N. Neurology. (1999) 53:846-51.
W39C	CMT1	8.7	Parental mosaicism of a novel PMP22 mutation with a minimal neuropathic phenotype. Taioli F, Bertolasi L, Ajena D, Ferrarini M, Cabrini I, Crestanello A, Fabrizi GM. J Peripher Nerv Syst. (2012) 17:414-7.
A67T*	HNPP	39.9	HNPP due to a novel missense mutation of the PMP22 gene. Nodera H, Nishimura M, Logigian EL, Herrmann DN, Kaji R. Neurology. (2003) 60:1863-4.
A67P*	CMT1 and deafness	24	A unique point mutation in the PMP22 gene is associated with Charcot-Marie-Tooth disease and deafness. Kovach MJ, Lin JP, Boyadjiev S, Campbell K, Mazzeo L, Herman K, Rimer LA, Frank W, Llewellyn B, Jabs EW, Gelber D, Kimonis VE. Am J Hum Genet. (1999) 64:1580-93.

PMP22 Mutation	Phenotype	Average Reported Motor Nerve Conduction Velocity (m/s)	Reference
M69R	CMT1	<1	Variable phenotypes are associated with PMP22 missense mutations. Russo M, Laurá M, Polke JM, Davis MB, Blake J, Brandner S, Hughes RA, Houlden H, Bennett DL, Lunn MP, Reilly MM. Neuromuscul Disord. (2011) 21:106-14.
M69K	DSS	3.3	Dejerine-Sottas syndrome associated with point mutation in the peripheral myelin protein 22 (PMP22) gene. Roa BB, Dyck PJ, Marks HG, Chance PF, Lupski JR. Nat Genet. (1993) 5:269-73.
L71P	CMT1/DSS + vestibular hearing loss	2-3	Charcot-Marie-Tooth disease and related neuropathies: mutation distribution and genotype-phenotype correlation. Boerkoel CF, Takashima H, Garcia CA, Olney RK, Johnson J, Berry K, Russo P, Kennedy S, Teebi AS, Scavina M, Williams LL, Mancias P, Butler IJ, Krajewski K, Shy M, Lupski JR. Ann Neurol. (2002) 51:190-201.
S72L	CMT1/DSS (+deafness)	4.3	Dejerine-Sottas neuropathy and PMP22 point mutations: a new base pair substitution and a possible "hot spot" on Ser72. Marques W Jr, Thomas PK, Sweeney MG, Carr L, Wood NW. Ann Neurol. (1998) 43:680-3. Dejerine-Sottas syndrome associated with point mutation in the peripheral myelin protein 22 (PMP22) gene. Roa BB, Dyck PJ, Marks HG, Chance PF, Lupski JR. Nat Genet. (1993) 5:269-73. Congenital hypomyelination neuropathy with Ser72Leu substitution in PMP22. Simonati A, Fabrizi GM, Pasquinelli A, Taioli F, Cavallaro T, Morbin M, Marcon G, Papini M, Rizzuto N. Neuromuscul Disord. (1999) 9:257-61. Infantile demyelinating neuropathy associated with a de novo point mutation on Ser72 in PMP22 and basal lamina onion bulbs in skin biopsy. Ceuterick-de Groote C, De Jonghe P, Timmerman V, Van Goethem G, Löfgren A, Ceulemans B, Van Broeckhoven C, Martin JJ. Pathol Res Pract. (2001) 197:193-8. Charcot-Marie-Tooth disease and related neuropathies: mutation distribution and genotype-phenotype correlation. Boerkoel CF, Takashima H, Garcia CA, Olney RK, Johnson J, Berry K, Russo P, Kennedy S, Teebi AS, Scavina M, Williams LL, Mancias P, Butler IJ, Krajewski K, Shy M, Lupski JR. Ann Neurol. (2002) 51:190-201. The range of chronic demyelinating neuropathy of infancy: a clinico-pathological and genetic study of 15 unrelated cases. Planté-Bordeneuve V, Parman Y, Guiochon-Mantel A, Alj Y, Deymeer F, Serdaroglu P, Eraksoy M, Said G. J Neurol. (2001) 248:795-803. Dejerine-Sottas' neuropathy caused by the missense mutation PMP22 Ser72Leu. Marques W Jr, Neto JM, Barreira AA. Acta Neurol Scand. (2004) 110:196-9. Dejerine-Sottas disease with de novo dominant point mutation of the PMP22 gene. Ionasescu VV, Ionasescu R, Searby C, Neahring R. Neurology. (1995) 45:1766-7.

PMP22 Mutation	Phenotype	Average Reported Motor Nerve Conduction Velocity (m/s)	Reference
			Dejerine-Sottas disease with sensorineural hearing loss, nystagmus, and peripheral facial nerve weakness: de novo dominant point mutation of the PMP22 gene. Ionasescu VV, Searby C, Greenberg SA. J Med Genet. (1996) 33:1048-9.
S72W	DSS	0	Hereditary demyelinating neuropathy of infancy. A genetically complex syndrome. Tyson J, Ellis D, Fairbrother U, King RH, Muntoni F, Jacobs J, Malcolm S, Harding AE, Thomas PK. Brain. (1997) 120 (Pt 1):47-63.
S76I	DSS+deafness	3	Variable phenotypes are associated with PMP22 missense mutations. Russo M, Laurá M, Polke JM, Davis MB, Blake J, Brandner S, Hughes RA, Houlden H, Bennett DL, Lunn MP, Reilly MM. Neuromuscul Disord. (2011) 21:106-14. Hereditary demyelinating neuropathy of infancy. A genetically complex syndrome. Tyson J, Ellis D, Fairbrother U, King RH, Muntoni F, Jacobs J, Malcolm S, Harding AE, Thomas PK. Brain. (1997) 120 (Pt 1):47-63.
S79C	CMT1	13.9	Charcot-Marie-Tooth disease type 1A. Association with a spontaneous point mutation in the PMP22 gene. Roa BB, Garcia CA, Suter U, Kulpa DA, Wise CA, Mueller J, Welcher AA, Snipes GJ, Shooter EM, Patel PI, Lupski JR. N Engl J Med. (1993) 329:96-101.
L80p	DSS	0	Hereditary demyelinating neuropathy of infancy. A genetically complex syndrome. Tyson J, Ellis D, Fairbrother U, King RH, Muntoni F, Jacobs J, Malcolm S, Harding AE, Thomas PK. Brain. (1997) 120 (Pt 1):47-63.
G93R	CMT1	17	HNPP due to a novel missense mutation of the PMP22 gene. Nodera H, Nishimura M, Logigian EL, Herrmann DN, Kaji R. Neurology. (2003) 60:1863-4.
G100E	DSS	<1	Variable phenotypes are associated with PMP22 missense mutations. Russo M, Laurá M, Polke JM, Davis MB, Blake J, Brandner S, Hughes RA, Houlden H, Bennett DL, Lunn MP, Reilly MM. Neuromuscul Disord. (2011) 21:106-14.
G107V	CMT1	22.7	A novel point mutation in the peripheral myelin protein 22 (PMP22) gene associated with Charcot-Marie-Tooth disease type 1A. Marrosu MG, Vaccargiu S, Marrosu G, Vannelli A, Cianchetti C, Muntoni F. Neurology. (1997) 48:489-93.
C109R	DSS	3.6	PMP22 related congenital hypomyelination neuropathy. Fabrizi GM, Simonati A, Taioli F, Cavallaro T, Ferrarini M, Rigatelli F, Pini A, Mostacciuolo ML, Rizzuto N. J Neurol Neurosurg Psychiatry. (2001) 70:123-6.
T118M	HNPP	37.9	Variable phenotypes are associated with PMP22 missense mutations. Russo M, Laurá M, Polke JM, Davis MB, Blake J, Brandner S, Hughes RA, Houlden H, Bennett DL, Lunn MP, Reilly MM. Neuromuscul Disord. (2011) 21:106-14. Evidence for a recessive PMP22 point mutation in Charcot-Marie-Tooth disease type 1A. Roa BB, Garcia CA, Pentao L, Killian JM, Trask BJ, Suter U, Snipes GJ, Ortiz-Lopez R, Shooter EM, Patel PI, Lupski JR. Nat Genet. (1993) 5:189-94.
S131C	HNPP/CMT1	37.3	Variable phenotypes are associated with PMP22 missense mutations.

PMP22 Mutation	Phenotype	Average Reported Motor Nerve Conduction Velocity (m/s)	Reference
			Russo M, Laurá M, Polke JM, Davis MB, Blake J, Brandner S, Hughes RA, Houlden H, Bennett DL, Lunn MP, Reilly MM. Neuromuscul Disord. (2011) 21:106-14.
I137V	Healthy poly-morphism	*Assumed 50+	Mutational analysis of the MPZ, PMP22 and Cx32 genes in patients of Spanish ancestry with Charcot-Marie-Tooth disease and hereditary neuropathy with liability to pressure palsies. Bort S, Nelis E, Timmerman V, Sevilla T, Cruz-Martínez A, Martínez F, Millán JM, Arpa J, Vílchez JJ, Prieto F, Van Broeckhoven C, Palau F. Hum Genet. 1997 99:746-54.
S149R	DSS	0	Dejerine-sottas disease with a novel de novo dominant mutation, Ser 149 Arg, of the peripheral myelin protein 22. Ohnishi A, Yamamoto T, Izawa K, Yamamori S, Takahashi K, Mega H, Jinnai K. Acta Neuropathol. (2000) 99:327-30.
G150D	DSS	<5	Dejerine-Sottas neuropathy in mother and son with same point mutation of PMP22 gene. Ionasescu VV, Searby CC, Ionasescu R, Chatkupt S, Patel N, Koenigsberger R. Muscle Nerve. (1997) 20:97-9.